We are IntechOpen, the world's leading publisher of Open Access books Built by scientists, for scientists

6,900
Open access books available

185,000
International authors and editors

200M
Downloads

Our authors are among the

154
Countries delivered to

TOP 1%
most cited scientists

12.2%
Contributors from top 500 universities



WEB OF SCIENCE™

Selection of our books indexed in the Book Citation Index in Web of Science™ Core Collection (BKCI)

Interested in publishing with us?
Contact book.department@intechopen.com

Numbers displayed above are based on latest data collected.
For more information visit www.intechopen.com



Chapter 7

Mixtures Composed of Liquid Crystals and Nanoparticles

Vlad Popa-Nita, Valentin Barna, Robert Repnik and Samo Kralj

Additional information is available at the end of the chapter

http://dx.doi.org/10.5772/50896

1. Introduction

The past decade has witnessed an increased interest in the study of mixtures [1–3] of various soft materials and nanoparticles. A characteristic feature of a nanoparticle is that at least one of its dimensions is limited to between 1 and 100 nm. It is of interest to find combinations where each component introduces a qualitatively different behavior into the system. Such systems are expected to play an important role in the emerging field of nanotechnology and also in composites with extraordinary material properties.

In several cases various liquid crystalline phases [4] are chosen as a soft carrier matrix. Their main advantageous properties are as follows. LCs are optically anisotropic and transparent. Their structure can be readily controlled by the confining surfaces and by applying an external electric or magnetic field. LCs exhibit a rich pallet of different structures and phases that can display almost all physical phenomena. In addition the chemistry of LCs is relatively well developed, which can mean the synthesis of LC molecules with the desired properties. As a result of these properties, even pure LC systems have found several applications, in particular in the electro-optics industry.

In our study we will confine our interest to the nematic LC phase formed by rod-like anisotropic molecules. The molecules tend to be parallel, at least locally. In bulk equilibrium nematic phase LC molecules are on the average aligned homogeneously along a single symmetry breaking direction, while translational ordering is absent. In thermotropic LCs nematic ordering is reached from the isotropic (ordinary liquid) phase by lowering the temperature via a weakly first order phase transition. Reversely, in lyotropic LCs the nematic ordering could be obtained via a first order phase transition by increasing packing density of LC molecules .

INTECH
open science | open minds

© 2013 Popa-Nita et al.; licensee InTech. This is an open access article distributed under the terms of the Creative Commons Attribution License (http://creativecommons.org/licenses/by/3.0), which permits unrestricted use, distribution, and reproduction in any medium, provided the original work is properly cited.

Various NPs are added to LC matrices in order to introduce additional quality into the system. It has been shown that in such mixtures one can obtain dramatically enhanced [2] or even new material properties [5] (e.g., multiferroics), which is of particular interest for composite materials with exceptional properties. Because the LC phases are reached via continuous symmetry-breaking phase transitions, the presence of NPs can stabilize the LC domain structures and consequently give rise to topological defects [3]. These can strongly interact with NPs, yielding different patterns that depend on the conditions at the LC-molecule-NP interface.

In several studies one uses as NPs carbon nanotubes (CNTs) [6–12]. Most of CNTs extraordinary properties of potential use in various applications could be realized in relatively well aligned samples. Recently it has been shown that liquid crystal alignment could trigger spontaneous ordering of CNTs with remarkably high degree of ordering [9–12]. CNTs orient parallel to average direction of liquid crystal (LC) alignment with an orientational order parameter between 0.6 to 0.9 [13–16]. Both, thermotropic [13, 14, 16] and lyotropic nematic LC phases [15] have been successfully applied as aligning solvents.

The theoretical study of the collective behavior of anisotropic nanoparticles dispersed in isotropic solvents or in liquid crystals is based on the observation that they can be consider essentially as rigid-rod polymers with a large aspect ratio [17]. The Onsager's theory for the electrostatic repulsion of long rigid rods has been used to investigate the phase behavior of SWNTs dispersed into organic and aqueous solvents [18]. In a good solvent, when the van der Waals attractive interaction between CNTs is overcome by strong repulsive interrods potential, the ordered phases of CNTs can form at room temperature. On the contrary, if the solvent is not good, the van der Waals attractive interactions between the rods are strong and as a result, only extremely dilute solutions of SWNTs are thermodynamically stable and no liquid crystal phases form at room temperature. The liquid crystallinity of CNTs with and without van der Waals interactions has been analyzed by using the density functional theory [19]. In the presence of van der Waals interaction, the nematic as well as the columnar phases occur in the temperature-packing fraction phase diagram in a wide range of very high temperatures. In the absence of van der Waals interaction, with an increase of packing fraction, the system undergoes an isotropic-nematic phase transition via a biphasic region. The isotropic-nematic packing fraction decreases with the increase of the aspect ratio of CNTs. To describe the dispersion of SWNTs in superacids, the Onsager theory for rigid rods was extended to include the length polydispersity and solvent mediated attraction and repulsion [20]. The main conclusion of these theoretical models is that to obtain liquid crystal phases of CNTs at room temperature the strong van der Waals interaction between them must be screened out. This requires a good solvent with an ability to disperse CNTs down to the level of individual tube.

In the previous papers [6–8] we have presented a phenomenological theory for predicting the alignment of length monodisperse CNTs dispersions in thermotropic nematic liquid crystals. We combined the Landau-de Gennes free energy for thermotropic ordering of the liquid crystal solvent and the Doi free energy for the lyotropic nematic ordering of CNTs caused by excluded-volume interactions between them. In the first paper [6], the interaction between CNTs and liquid crystal molecules is thought to be sufficiently weak to not cause any director field deformations in the nematic host fluid. The principal results of this first study could be summarized as follows. (i) The coupling between the CNTs and a LC seems to be dominated by an anisotropic surface tension not by any deformation of the director field because the

http://dx.doi.org/10.5772/50896

rods are thin on the scale of the extrapolation length. This means that CNTs dispersed in NLCs are in the weak-anchoring limit. (ii) The first order nematic-isotropic phase transition of CNTs dispersed in a LC disappears for a strong enough coupling to the nematic host fluid. A tricritical point can be defined that within the Landau-de Gennes model exhibits universal characteristics if expressed in the right dimensionless variables. (iii) Although in the weak-anchoring limit, the coupling between the CNTs and the LC host is so strong that in practice one should expect CNTs always to be in the strong-coupling limit, i.e., above the tricritical point. This means CNTs in LCs are always strongly paranematic. (iv)The degree of alignment of CNTs in NLCs can be tuned by varying the CNT concentration or the temperature.

The phase and structural behavior of a mixture of CNT and LC using a mean field-type phenomenological model in the strong anchoring regime was presented in the second paper [7]. We have considered cases where the nematic director field is either nonsingular or where topological defects are present in the LC medium. The effective field experienced by CNTs yields pretransitional ordering below the critical point. Above the critical point, a gradual variation of orientational order of CNTs appears. In practice one should expect CNTs always to be in the strong-coupling limit, i.e., far above the critical point. This means CNTs in the nematic phase of LC are always strongly paranematic. The model predicts an increase of nematic-isotropic phase transition temperature of LC with the volume fraction of CNTs as well as the presence of a triple point in the phase diagram. For realistic values of the coupling constant, the degree of ordering of CNTs is enslaved by the properties of the host nematic fluid.

The comparison of the results for weak anchoring and strong anchoring regimes, respectively was presented in the third paper [8]. In both anchoring cases, the first-order nematic - isotropic phase transition of CNTs dispersed in the nematic phase transforms into a continuous transition for a strong enough coupling to the nematic host fluid. The corresponding critical value of the coupling parameter increases with increasing temperature being larger in the strong anchoring limit case. The numerical estimate of the coupling constants in the two anchoring regimes indicates that the coupling is so strong that CNTs are far above the critical point, meaning that the nematic-isotropic phase transition is a continuous one. In both cases, we have plotted the phase diagram of the homogeneous mixture for the same value of the coupling parameter. In both cases, three regions of the phase diagram could be distinguished and correspondingly the existence of triple points are shown. We mention that in both anchoring cases, the nematic-isotropic phase transition temperature of LC increases with the volume fraction of CNTs, a well-known experimental result.

Usually, after the acid treatment and ultrasonication (to enhance the dispersion and stability of the CNTs suspensions), depending on the temperature of water bath and time of ultrasonication, the obtained CNTs have different lengths and diameters [14, 21]. The influence of length bidispersity on the phase diagram and alignment of CNTs is the subject of the present paper. As the first step we extend our mesoscopic model [6–8] and consider length bidispersity of CNTs. We mention that the effect of bidispersity of the long rigid rods has been discussed in the framework of Onsager theory [22–25]. We shall refer to their results in the last section of the paper.

The plan of the paper is as follows. In the first part of the paper we focus on mixtures of nematic LCs and isotropic NPs. A simple phenomenological model is used which is sufficient to identify key mechanisms which might trigger phase separation. Conditions for efficient trapping of NPs to cores of topological defects is discussed. In the second part we confine our interest to mixtures of nematic LCs and carbon nanotubes. Using a simple model we take into account length dispersity of CNTs and analyze corresponding phase diagrams. In the last section we summarize the main results.

2. Binary nematogen - nonnematogen mixtures

We first consider a mixture of nematic LC and isotropic NPs using a relatively simple phenomenological model. We identify key phase separation triggering mechanisms. We also discuss conditions enabling efficient trapping of NPs within cores of topological defects or strongly localized elastic distortions. If these trapping sites are relatively uniformly spatially distributed they might prevent phase separation.

2.1. Free energy

We use semiphenomenological model within which the volume concentration of isotropic NPs is given by the conserved parameter ϕ. The orientational order of LC molecules is described by the symmetric and traceless tensor order parameter [4] $Q = \sum_{i=1}^{3} \lambda_i \overrightarrow{e}_i \otimes \overrightarrow{e}_i$, where λ_i and $\overrightarrow{e}_i$ stand for its eigenvalues and corresponding eigenvectors, respectively. In the case of uniaxial ordering Q is commonly expressed in terms of the nematic director field $\overrightarrow{n}$ and the uniaxial orientational order parameter S as [4]

$$Q = S\left(\overrightarrow{n} \otimes \overrightarrow{n} - \frac{1}{3} I\right). \tag{1}$$

Here I stands for the identity tensor. The unit vector $\overrightarrow{n}$ points along the local uniaxial ordering direction, where states $\pm\overrightarrow{n}$ are equivalent (the so called head-to-tail invariance). The extent of fluctuations is determined by S, where $S = 1$ and $S = 0$ reflect rigid alignment along $\overrightarrow{n}$ and isotropic liquid ordering, respectively. If strong distortions are present biaxial states could be locally entered. Degree of biaxiality is assessed via parameter [26]

$$\beta^2 = 1 - \frac{6(trQ^3)^2}{(trQ^2)^3}, \tag{2}$$

ranging in the interval $[0, 1]$. Uniaxial configurations correspond to $\beta^2 = 0$ and an ordering with the maximum degree of biaxiality is signaled by $\beta^2 = 1$.

The free energy F of a mixture is expressed as

$$F = \int \left(f_m + f_c + f_e + f_i \delta(\overrightarrow{r} - \overrightarrow{r}_i)\right) d^3\overrightarrow{r}. \tag{3}$$

The quantity δ stands for the delta measure, $\overrightarrow{r}_i$ locates NP-LC interfaces and the integral runs over the LC volume. The role of different contributions in Eq.(3) is as follows.

http://dx.doi.org/10.5772/50896

The mixing term f_m describes the isotropic mixing of the two components. Within the Flory theory [27] it is expressed as

$$f_m = \frac{k_B T}{v_{lc}}(1-\phi)\ln(1-\phi) + \frac{k_B T}{v_{np}}\phi\ln\phi + \chi\phi(1-\phi). \tag{4}$$

Here k_B is the Boltzmann constant, T is the absolute temperature, and χ stands for the Flory-Huggins parameter [27]. The volume of a LC molecule and of a nanoparticle is given by v_{lc} and v_{np}, respectively,

The condensation contribution f_c enforces orientational LC ordering below a critical temperature T_{NI}. Is is expressed as [4]

$$f_c = \frac{3a(T-T^*)}{2}Q_{ij}Q_{ij} - \frac{9B}{2}Q_{ij}Q_{jk}Q_{kj} + \frac{9C}{4}(Q_{ij}Q_{ij})^2, \tag{5}$$

where summation over repeated indices is assumed. The quantities a, B, C, are material constants and T^* denotes the spinodal temperature limit of the isotropic phase of the pure LC. This condensation free energy term describes a weakly first order nematic-isotropic phase transition. At $T = T_{NI} = T^* + B^2/(4aC)$, the two phases, nematic ($S^{(NI)} = B/(2C)$) and isotropic ($S = 0$) coexist in equilibrium.

The deviations from homogeneous nematic ordering are penalized by the elastic term

$$f_e = \frac{L}{2}Q_{jk,i}Q_{jk,i}, \tag{6}$$

which is expressed within a single elastic constant approximation. Here L is the representative bare nematic elastic constant.

The conditions at the NP-LC interface are determined by the term f_i. We express it as

$$f_i = -we_k Q_{kj} e_j, \tag{7}$$

where $w > 0$ is the anchoring strength favoring the nematic ordering at an interface and $\overrightarrow{e}$ stands for the local surface normal.

2.2. Phase separation tendency

We proceed by identifying key mechanisms favoring phase separation tendency in a mixture of NPs and nematic liquid crystal. We describe global LC orientational ordering with a spatially averaged order parameter $\overline{S}$ and volume concentration of nanoparticles $\overline{\phi}$. Here the over-bar $\overline{(..)}$ denotes the spatial average. Relative presence of NPs and LC molecules in the mixture is therefore given by $\overline{\phi} = N_{np}v_{np}/V$ and $1-\overline{\phi}$, respectively. Here N_{np} counts the number of NPs and V stands for the volume of the sample.

The resulting average free energy density is expressed as $\overline{f} = \overline{f}_m + \overline{f}_c + \overline{f}_e + \overline{f}_i$, where

$$\overline{f}_m \sim \frac{k_B T}{v_{lc}}(1-\overline{\phi})\ln(1-\overline{\phi}) + \frac{k_B T}{v_{np}}\overline{\phi}\ln\overline{\phi} + \chi\overline{\phi}(1-\overline{\phi}), \tag{8}$$

$$\overline{f}_c \sim \left(1-\overline{\phi}\right)\left(a(T-T^*)\overline{S}^2 - B\overline{S}^3 + C\overline{S}^4\right), \tag{9}$$

$$\overline{f}_e \sim \left(1-\overline{\phi}\right) L\overline{S}^2/\overline{\xi}_d^{\,2}, \tag{10}$$

$$\overline{f}_i \sim -\left(1-\overline{\phi}\right)\overline{\phi} w\overline{S}. \tag{11}$$

The factor $\left(1-\overline{\phi}\right)$ present in terms $\overline{f}_c$ and $\overline{f}_e$ accounts for the part of the volume not taken up by LC. Furthermore, the factor $\left(1-\overline{\phi}\right)\overline{\phi}$ in $\overline{f}_i$ accounts for absence of this term if $\overline{\phi}=0$ or $\overline{\phi}=1$. Note that in general $T^* = T_*(\phi)$. Simple binary modeling [28] suggests $T^* = T_0 - \lambda\overline{\phi}$, where T_0 and λ are positive material constants. It accounts for weaker interactions among LC molecules due to presence NPs. In general NPs could introduce spatially nonhomogeneous orientational ordering of LC molecules which is taken into account by $\overline{f}_e$. On average degree of elastic distortions in $\overrightarrow{n}$ is approximated by the average domain length $\overline{\xi_d}$.

From the expression for $\overline{f}$ one can extract the effective Flory-Huggins [27] parameter

$$\chi_{eff} = \chi + a\lambda\overline{S}^2 - w\overline{S}. \tag{12}$$

The phase transition takes place if χ_{eff} exceeds a threshold value χ_c. In typical LCs it holds [29] $\chi << a_0\lambda$ and $\chi < \chi_c$. Henceforth we limit our attention to such cases. Consequently, in the isotropic phase (where $\overline{S}=0$) homogeneous mixtures are established. On entering orientational ordered phase different scenaria can be realized. We first consider cases where the wetting interaction between LCs and NPs is negligible weak (i.e., $w \sim 0$). In this case phase separation is very likely. It is triggered providing $\chi + a\lambda\overline{S}^2 \sim a\lambda\overline{S}^2 > \chi_c$. However, strong enough surface wetting interaction could suppress phase separation providing $\chi + a\lambda\overline{S}^2 - w\overline{S} < \chi_c$.

Next, we consider cases where there exist localized regions in LC ordering exhibiting strong local distortions. Therefore, in some parts $\overline{\xi_d}$ entering the expression for $\overline{f}_e$ is relatively small. From Eq.(10) we infer that local free energy penalties could be reduced if they are occupied by NPs (i.e., $\overline{\phi} \sim 1$). Therefore, the structure of expression for $\overline{f}$ suggests that NPs tend to assemble at local elastic distortions in order to reduce the total free energy penalty of the system.

2.3. Interaction between NPs and topological defects

In this section we investigate in more detail interaction between NPs and localized elastic distortions. We estimate general conditions for which this interaction is attractive. For this purpose we study a specific example where we enforce a topological defect within a cell. We add NPs exhibiting different surface constraints and determine conditions for which attractive interaction is enabled.

http://dx.doi.org/10.5772/50896

We consider LC ordering within a cylindrical plane-parallel cell of thickness h and radius R. The cell is schematically depicted in Fig.1.

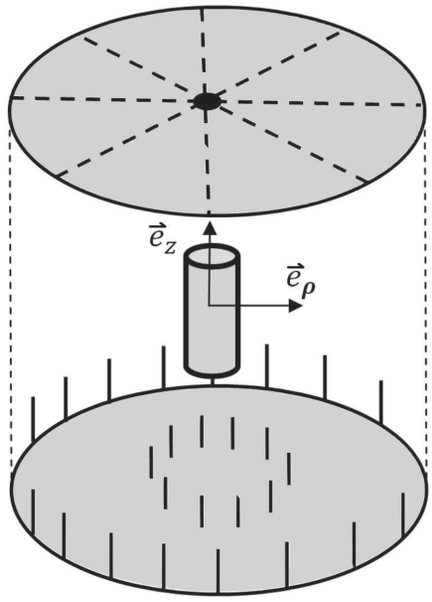


Figure 1. Schematic presentation of the hybrid plan-parallel cell hosting a nanoparticle at its symmetry axis. The diameter and the height of cylindrically shaped NP is in simulation set to be equal to the biaxial correlation length ξ_b. Furthermore, we set $h = 2R = 10\xi_b$, where h describes the height and R the radius of the cell.

We use the cylindrical coordinate system determined by unit vectors $\{\overrightarrow{e}_\rho, \overrightarrow{e}_\varphi, \overrightarrow{e}_z\}$. Here $\overrightarrow{e}_\rho$ is the radial unit vector, $\overrightarrow{e}_z$ points along the z-coordinate, while $\overrightarrow{e}_\varphi = \overrightarrow{e}_z \times \overrightarrow{e}_\rho$. We enforce a topological defect (boojum) [30] by imposing strong hybrid anchoring conditions at the confining plates. At the top plate ($z = h$) strong uniaxial radial anchoring is set imposed, i.e., we enforce $Q(z = h) = Q_{rad} \equiv S_{eq}\left(\overrightarrow{e}_\rho \otimes \overrightarrow{e}_\rho - \frac{1}{3}I\right)$. Here S_{eq} stands for the equilibrium nematic order parameter. At the bottom plate we impose strong homeotropic anchoring, i.e. $Q(z = h) = Q_{\text{hom}} \equiv S_{eq}\left(\overrightarrow{e}_z \otimes \overrightarrow{e}_z - \frac{1}{3}I\right)$. At the lateral wall we set free boundary conditions. The resulting equilibrium equations were solved numerically, where technical details are given in [30] and [31].

The boojum structure is well characterized by its biaxial spatial profile shown in Fig. 2.

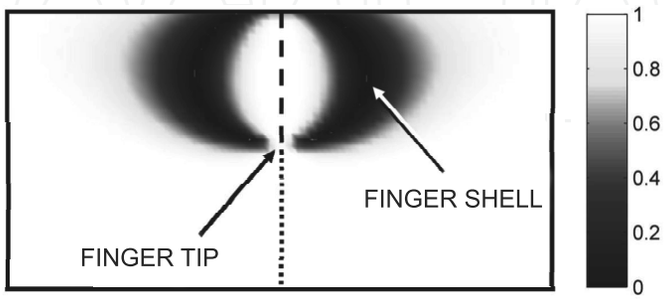


Figure 2. The cross-section through the boojum where we plot the degree of biaxiality β^2. A biaxial shell joins the isotropic finger tip and the upper surface. Along the cylindrical axis the system exhibits uniaxial ordering due to topological reasons (dashed line: negative uniaxiality, dotted line: positive uniaxiality). In the illustration the anchoring strength at the top plane is finite. The characteristic defect size is comparable to the biaxial correlation length. On the right side of the figure the grayscale bar of $1 - \beta^2$ is shown.

We plot $\beta^2(\rho, z)$ dependence (see Eq.(2)) in the plane through the defect core. Note that the system exhibits cylindrical symmetry. The boojum is characterized by a finger-like structure, where the finger tip is melted by topologically reasons. The boojum core structure is analyzed in detail in [30] and here we briefly summarize its main characteristics. The defect core is dominated by a *finger* protruding into the cell's interior along its symmetry axis. The center of the *finger*, residing at the cylinder axis, is negatively uniaxial ($S < 0$). It ends in a melted (isotropic) point ($S = 0$) to which we refer as the *finger tip*. It is placed roughly at the distance $\xi_f \sim \xi_b$ from the surface, where ξ_b stands for the biaxial correlation length. Below the *finger tip* the nematic configuration is positively uniaxial ($S > 0$) at the symmetry axis. The *finger* is enclosed within a biaxial shell exhibiting maximal biaxiality [26, 30] which joins the *finger* tip with the upper surface. By topological reasons the nematic order parameter melts only at the *finger tip* for realistic anchoring strengths. Note that in Fig. 2 the biaxial profile is plotted for a more realistic finite anchoring strength for which the finger-like profile is well pronounced.

At the cylinder axis we place a cylindrically shaped NP. The height and diameter of the NPs is set equal to ξ_b. Our interest is to estimate impact of NP surface treatment on interaction with its surrounding. For this purpose we impose three qualitatively different strong boundary conditions at the NP surface which is determined by the position vector $\overrightarrow{r}_i$: i) $Q(\overrightarrow{r}_i) = 0$, ii) $Q(\overrightarrow{r}_i) = Q_{rad}$, iii) $Q(\overrightarrow{r}_i) = Q_{\mathrm{hom}}$. These conditions locally enforce melting, radial, and spatially homogeneous configuration, respectively. We calculate the LC free energy within the cell as a function of the NP position along the z axis. Note that three qualitatively different areas exist within the cell. These are: i) region surrounding the melted point at the boojum *finger tip*, ii) prevailing radial ordering at $z \sim h$, and iii) the homogeneous ordering along $\overrightarrow{e}_z$ at $z \sim 0$. We vary the position of NP along the z-axis, and for each position we calculate the free energy of the system. In Fig. 3 we plot the total free energy as a function of z-coordinate for three different surface treatments.

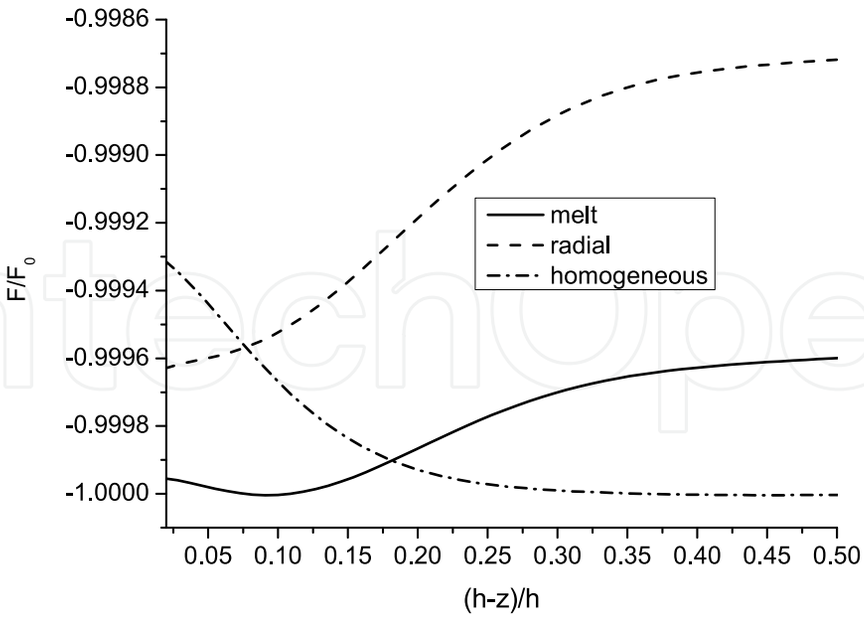


Figure 3. The free energy F of the system as a function of the nanoparticle position along the symmetry axis. The free energy is scaled with respect to the minimum of free energy F_0 calculated for the melted boundary condition. One sees that for the i) melted ii) radial and iii) homogeneous boundary condition the free energy exhibits minimum at i) the finger tip ii) $z = h$, iii) $z = 0$, respectively.

We see that NP enforcing i) melting, ii) radial, iii) homogeneous configuration tends to migrate towards the i) *finger tip*, ii) top plate, iii) bottom plate, respectively. Simulations shows that NPs tend to migrate towards regions which exhibit a similar local structure with respect to the conditions at the NP surface. Therefore, to assemble efficiently NPs at a defect core it is essential to make the surface coating such that the effective NP configuration resembles the defect core structure.

We next assume that NPs environment resembles a defect core structure and therefore tend to be trapped within the core of the defect. In the following we estimate the free energy gain if the NP is trapped within the core. For illustration we consider a line defect (disclination) of length h. Note that lattices of topological defects can be stabilized either by inherent LC property (e.g. chirality [3]) or imposed geometrically by imposing frustrating boundary conditions [32]. The corresponding condensation free energy penalty ΔF_c for introducing the defect line inside an orientational ordered medium is roughly given by

$$\Delta F_c \sim a(T_{NI} - T)\overline{S}^2 \pi \xi^2 h. \tag{13}$$

Here T_{NI} refers to I-N phase transition temperature and $T < T_{NI}$. The core average radius is roughly given by the relevant (uniaxial or biaxial) order parameter correlation length ξ. Within the core the LC order is either essentially melted (i.e. $S \sim 0$) or strongly biaxial [33].

We next assume that NPs are added to the LC medium and that they collect at the disclination line. If NPs do not apparently disrupt the defect core structure then the condensation free energy penalty is decreased due to the reduced volume occupied by the energetically costly essentially isotropic (or strongly biaxial) phase [34]. One refers to these effect as the *Defect Core Replacement mechanism* [3]. The resulting decrease in ΔF_c penalty reads

$$\Delta F_c() \sim a(T_{NI} - T)\overline{S}^2 \left(\pi \xi^2 h - N_{np}^{(def)} v_{np} \right), \tag{14}$$

where $N_{np}^{(def)}$ counts number of NPs trapped within the core.

3. Dispersions of carbon nanotubes

We next consider mixtures of nematic LCs and carbon nanotubes with length bidispersity. We furthermore assume homogeneous uniaxial orientational alignment of all components along a single symmetry breaking direction.

3.1. Free energy of three component mixtures

The mixture is characterized by the volume fractions of the three components:

$$\Phi_i = \frac{N_i v_i}{\sum_{i=1}^{3} N_j v_j} \quad \text{with} \quad \sum_{i=1}^{3} \Phi_i = 1, \tag{15}$$

where N_i is the number of molecules of component i ($i = 1$ defines the liquid crystal with molecules of length $L_{01} = 3$ nm and diameter $D_1 = 0.5$ nm, $i = 2$ the CNTs of length $L_{02} = 400$ nm and diameter $D = 2$ nm, and $i = 3$ the CNTs of length $L_{03} = 800$ nm and diameter $D = 2$ nm) and v_i is the volume of a particle of component i. For latter convenience we introduce scaled CNT lengths $L_i = L_{0i}/D$ ($i = 2, 3$).

The degree of alignment of every component of the mixture is characterized by the scalar order parameter S_i [4]. The corresponding isotropic liquid of the component i is characterized by $S_i = 0$ while a perfectly oriented nematic phase would correspond to $S_i = 1$.

The free energy per unit volume of the mixture is expressed as

$$f = f_{CNT} + f_{LC} + f_C, \tag{16}$$

where f_{CNT} describes contribution of the two CNT components dispersed in the LC fluid, f_{LC} represents the free energy density of nematic liquid crystal order, while f_C takes into account the coupling between LC molecules and CNTs, respectively.

The free energy density of CNTs is given by [6, 7]

$$\frac{f_{CNT}}{k_B T} = \sum_{i=1}^{3} \frac{\Phi_i}{v_i} \ln \Phi_i + \sum_{i=2}^{3} \frac{L_i \Phi_i^2}{6 v_i} \left[\left(\frac{3}{L_i \Phi_i} - 1 \right) S_i^2 - \frac{2}{3} S_i^3 + S_i^4 \right] - \frac{\gamma_{23}}{k_B T} \Phi_2 \Phi_3 S_2 S_3. \tag{17}$$

The first sum represents the entropic isotropic contribution due to mixing of the two CNT components and LC neglecting their orientational degree of ordering [27]. The second sum describes a first order orientational phase transition of the i-species of CNT from the isotropic phase with $S_i = 0$, to the nematic phase with $S_i = (1 + \sqrt{9 - 24/L_i \Phi_i})/4$. The first order nematic-isotropic phase transition takes place at $\Phi_i^{(NI)} = 2.7/L_i$ and $S_i^{(NI)} = 1/3$. It is obtained starting from the Onsager theory [35] and using the Smoluchovsky equation [36, 37]. The model neglects the van der Waals attractions between CNTs which are responsible for their tendency to form bundles. The last term in Eq. (17) represents the interaction energy between the different CNTs species, where the interaction parameter γ_{23} is given by

$$\gamma_{23} = 8 k_B T / \pi D^3 \approx 10^6 \text{ N/m}^2.$$

This expression for γ_{23} is obtained using the same Doi procedure [36, 37] starting with the Onsager theory for a bidisperse hard rods system.

The second term in Eq. (16) is the Landau-de Gennes free energy density [4] which describes the weakly first-order nematic-isotropic phase transition of thermotropic LC

$$f_{LC} = \Phi_1 [a(T - T^*) S_1^2 - B S_1^3 + C S_1^4]. \tag{18}$$

For representative LC material we chose pentylcyanobiphenyl (5CB), for which $T^* = 307.55$ K, $a \approx 5.2 \cdot 10^4$ J/m^{3}K, $B \approx 5.3 \cdot 10^5$ J/m^3, $C \approx 9.7 \cdot 10^5$ J/m^3 [38]. This choice yields $S_1^{(NI)} = 0.275$ and $T_{NI} = 308.95$ K.

The third term in Eq.(16) represents the coupling between the liquid crystal molecules and the two CNT species. The resulting coupling term structure in both anchoring limits (weak and strong) was estimated in [6, 7]. The two limits are defined by the ratio DW/K, where W is the anchoring energy of a LC-nanotube interface, K is the average Frank nematic elastic constant. For typical values of $D = 2$ nm, $K \approx 10^{-11}$ N, $W \approx 10^{-6}$ N/m, $DW/K << 1$. Consequently, only the weak-anchoring limit needs to be considered, as already concluded by Lynch and Patrick [13]. The corresponding free energy density of coupling is approximately given by [6]:

$$f_C = -\gamma_{12}\Phi_2 S_1 S_2 \left(1 - \frac{1}{2}S_2\right) - \gamma_{13}\Phi_3 S_1 S_3 \left(1 - \frac{1}{2}S_3\right). \tag{19}$$

The terms in brackets ensures that $S_i \to 1$ when $\gamma_{12}(\gamma_{13}) \to \infty$ as it should. The coupling parameters γ_{12} and γ_{13} depend only on the anchoring energy of CNTs at the LC molecules surface and the diameter of CNTs [6] (no on their lengths). Therefore

$$\gamma_{12} = \gamma_{13} = \gamma_1 = 4W/3D \approx 10^3 \text{ N/m}^2$$

and the coupling free energy can be written as

$$f_C = -\gamma_1 S_1 \left[\Phi_2 S_2 \left(1 - \frac{1}{2}S_2\right) + \Phi_3 S_3 \left(1 - \frac{1}{2}S_3\right)\right]. \tag{20}$$

The free energy per unit volume of a monodisperse system (one species of CNTs of the diameter D and length L_{02} ($L_2 = L_{02}/D$, the volume v_2 and the volume fraction Φ) dispersed in a LC (with the molecular volume v_1 and the volume fraction $1 - \Phi$) is given by

$$\begin{aligned} f = {} & k_B T \left[\frac{1-\Phi}{v_1}\ln(1-\Phi) + \frac{\Phi}{v_2}\ln\Phi\right] \\ & + k_B T \frac{L_2\Phi^2}{6v_2}\left[\left(\frac{3}{L_2\Phi_2} - 1\right)S_2^2 - \frac{2}{3}S_2^3 + S_2^4\right] \\ & + (1-\Phi)[a(T-T^*)S_1^2 - BS_1^3 + CS_1^4] - \gamma_1\Phi S_1 S_2\left(1 - \frac{1}{2}S_2\right). \end{aligned} \tag{21}$$

3.2. Equilibrium equations

In the bidisperse case, the equilibrium values of the order parameters are obtained by minimization of the free energy density (Eqs. (16), (17), (18), and (19))with respect to S_1, S_2, and S_3, respectively. From the corresponding equations we find the equilibrium values of the order parameters in the nematic phase ($S_{i\text{n}}$) and paranematic phase ($S_{i\text{p}}$), respectively. Once the minimization procedure has been solved the volume fractions of the coexisting phases are found by solving the equilibrium conditions:

$$\mu_2(S_{1n}, S_{2n}, S_{3n}, \Phi_{2n}, \Phi_{3n}) = \mu_2(S_{1p}, S_{2p}, S_{3p}, \Phi_{2p}, \Phi_{3p}),$$
$$\mu_3(S_{1n}, S_{2n}, S_{3n}, \Phi_{2n}, \Phi_{3n}) = \mu_3(S_{1p}, S_{2p}, S_{3p}, \Phi_{2p}, \Phi_{3p}),$$
$$g(S_{1n}, S_{2n}, S_{3n}, \Phi_{2n}, \Phi_{3n}) = g(S_{1p}, S_{2p}, S_{3p}, \Phi_{2p}, \Phi_{3p}), \quad (22)$$

where the chemical potential of the two species of CNTs μ_2, μ_3, and the grand potential g are defined by the equations

$$\mu_2 = \frac{\partial f}{\partial \Phi_2}; \;\; \mu_3 = \frac{\partial f}{\partial \Phi_3}; \;\; g = f - \mu_2\Phi_2 - \mu_3\Phi_3. \quad (23)$$

There are three equilibrium equations with four variables: Φ_{2n}, Φ_{3n}, Φ_{2p}, and Φ_{2p}. We take Φ_{3p} as freely variable and calculate the other three Φ_{2n}, Φ_{3n}, Φ_{2p} from the coexistence equations (22).

In the monodisperse case, the equilibrium values of the order parameters (S_{1p}, S_{2p}, S_{1n}, and S_{2n})are obtained minimizing the free energy (21) with respect to S_1 and S_2 and the equilibrium conditions are given by

$$\mu(S_{1n}, S_{2n}, \Phi_n) = \mu(S_{1p}, S_{2p}, \Phi_p),$$
$$g(S_{1n}, S_{2n}, \Phi_n) = g(S_{1p}, S_{2p}, \Phi_p), \quad (24)$$

where the chemical potential of CNTs and the grand potential are defined as: $\mu = \partial f/\partial\Phi$, and $g = f - \mu\Phi$, respectively.

3.3. Phase behavior

In the first part of this section we present the phase behavior of monodisperse CNTs immersed in LC as a function of T, Φ and γ_1, while in the last part the analyze of the phase behavior of the bidisperse system is analyzed as a function of T, Φ_2, Φ_3 and γ_1.

3.3.1. Monodisperse CNTs

The coupling term between CNTs and the LC molecules in (21) induces two different region in the phase diagram separated by a critical line $\gamma_1^{(c)}(T)$. i) For $\gamma_1 < \gamma_1^{(c)}$, the CNTs exhibit a first order (discontinuous) phase transition between a paranematic phase (a phase with a low degree of orientational order) and a nematic phase (the *subcritical* region). ii) On the contrary, for $\gamma_1 > \gamma_1^{(c)}$, CNTs display gradual variation of S_2 with Φ (the *supercritical* regime).

The critical line $\gamma_1^{(c)}(T)$ is obtained by solving the equations $\partial f/\partial S_1 = \partial f/\partial S_2 = \partial^2 f/\partial S_2^2 = \partial^3 f/\partial S_2^3 = 0$. They yield at the critical point universal values for the order parameter $S_2^{(c)} = 1/6$ and volume fraction $\Phi^{(c)} = 18/7L_2$. The $\gamma_1^{(c)}(T)$ dependence for the two species of CNTs is presented in Figure 4.

http://dx.doi.org/10.5772/50896

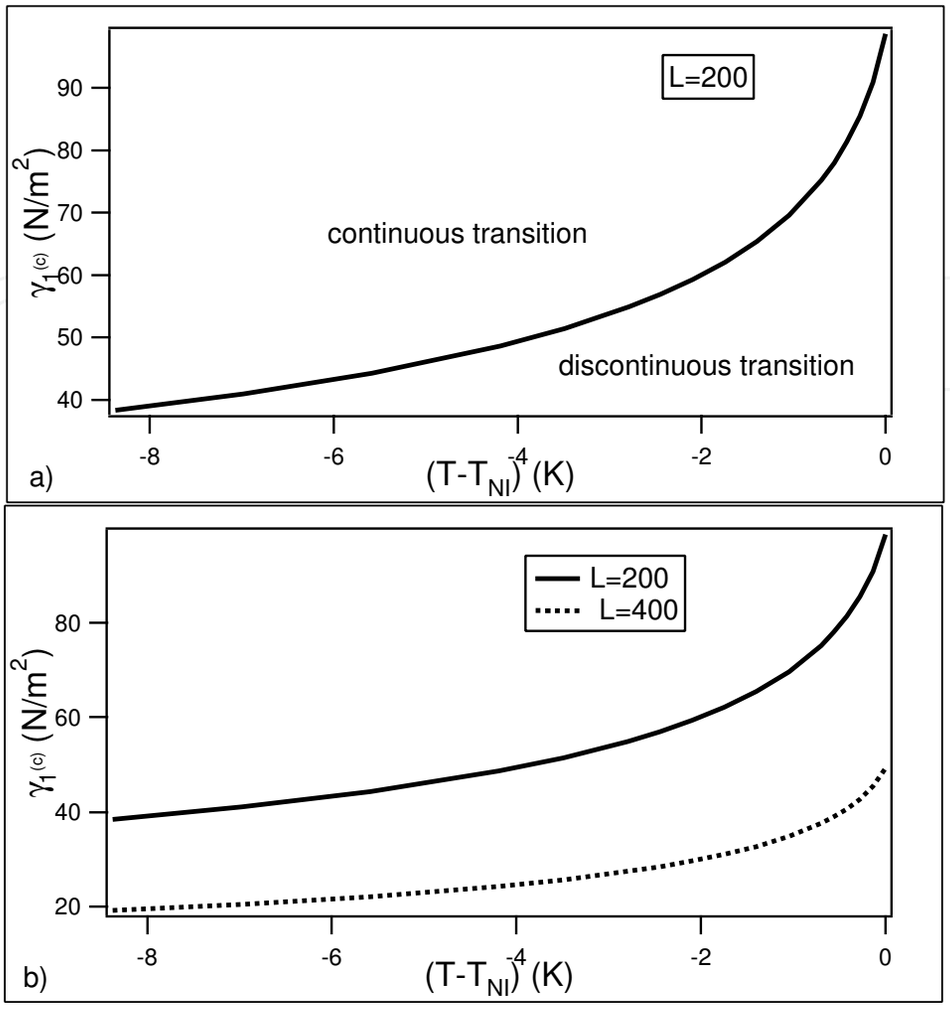


Figure 4. The critical value of the coupling parameter $\gamma_1^{(c)}$ as function of temperature calculated for both species of CNTs in the nematic LC phase.

On decreasing the temperature the external field felt by the CNTs is increasing due to increasing value of S_1 and the nematic-isotropic phase transition of CNTs becomes gradual for lower values of interaction parameter $\gamma_1^{(c)}$. Furthermore, the critical value of γ_1 decreases with increasing the length of CNTs. Therefore, the continuity of paranematic-nematic phase transition is favored by longer CNTs.

The phase diagram for the monodisperse system in the *subcritical* regime, for $L_2 = 200$ and $L_2 = 400$, respectively is shown in Figure 5.

Depending on temperature, we distinguish two regions in the phase diagram: i) for $T < T_{NI}$, the LC is in the nematic phase and the CNTs exhibit a first order phase transition with increasing Φ from a paranematic to a nematic phase. With decreasing temperature, the order parameter jump ($S_{2n} - S_{2p}$) as well as the difference in the volume fractions ($\Phi_n - \Phi_p$) become lower and they cancel at some temperature lower for shorter CNTs. This is due to the fact that the value of $\gamma_1 = 40.33$ N/m^2 considered, corresponds to a critical temperature $T - T_{NI} = -7.31$ K for shorter CNTs ($L_2 = 200$) and $T - T_{NI} = -0.45$ K for longer CNTs ($L_2 = 400$), respectively. We emphasize that the longer CNTs become ordered at lower

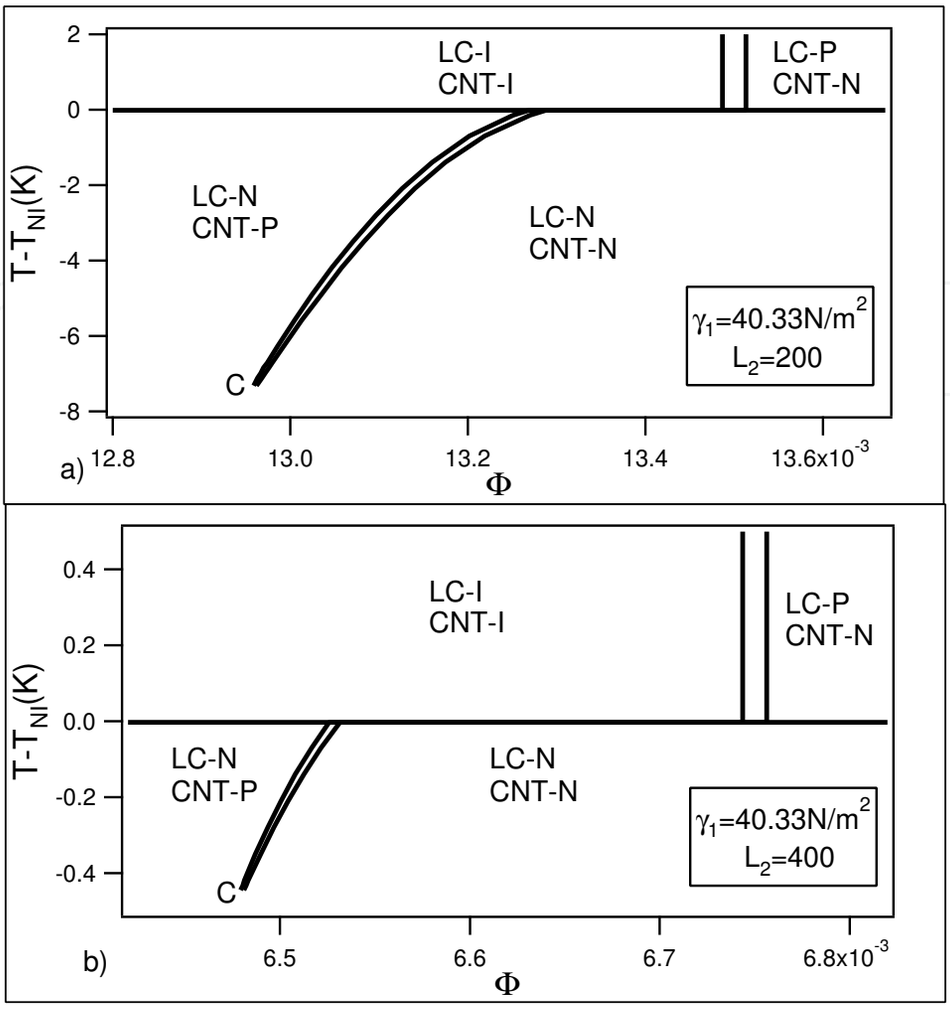


Figure 5. The (T, Φ) phase diagram of a monodisperse system in the *subcritical* regime. I means isotropic, P-paranematic, and N-nematic.

volume fraction. ii) for $T > T_{NI}$, the LC is in the isotropic phase ($S_1 = 0$) and the volume fraction gap of CNTs at the transition does not depend on temperature (the Flory horn [27]). Again the longer CNTs become aligned at lower volume fractions. It is important to note also the influence of CNTs on the LC alignment in this region. Above T_{NI}, the transition of CNTs from isotropic to nematic induces the transition of LC from isotropic to a paranematic phase (with a very very small degree of ordering for this value of the coupling constant). This problem of the influence of LC properties by the CNTs is not elucidated neither theoretically, nor experimentally yet and will be a subject of a future study.

To see in more detail the orientational order developed in the system, we have plotted in Figures 6 and 7 the order parameter variation as a function of the volume fraction Φ of the CNTs at a fixed temperature.

In Figure 6a, the temperature corresponds to a *subcritical* regime ($\gamma_1 < \gamma_1^{(c)}$) (see Figure 4), and the transition of CNTs is a discontinuous one with a jump in the order parameter. On the contrary, the temperature in Figure 6b corresponds to a *supercritical* regime because for this temperature $\gamma_1 > \gamma_1^{(c)}$ (see Figure 4). As a consequence, the CNTs phase transition is

http://dx.doi.org/10.5772/50896

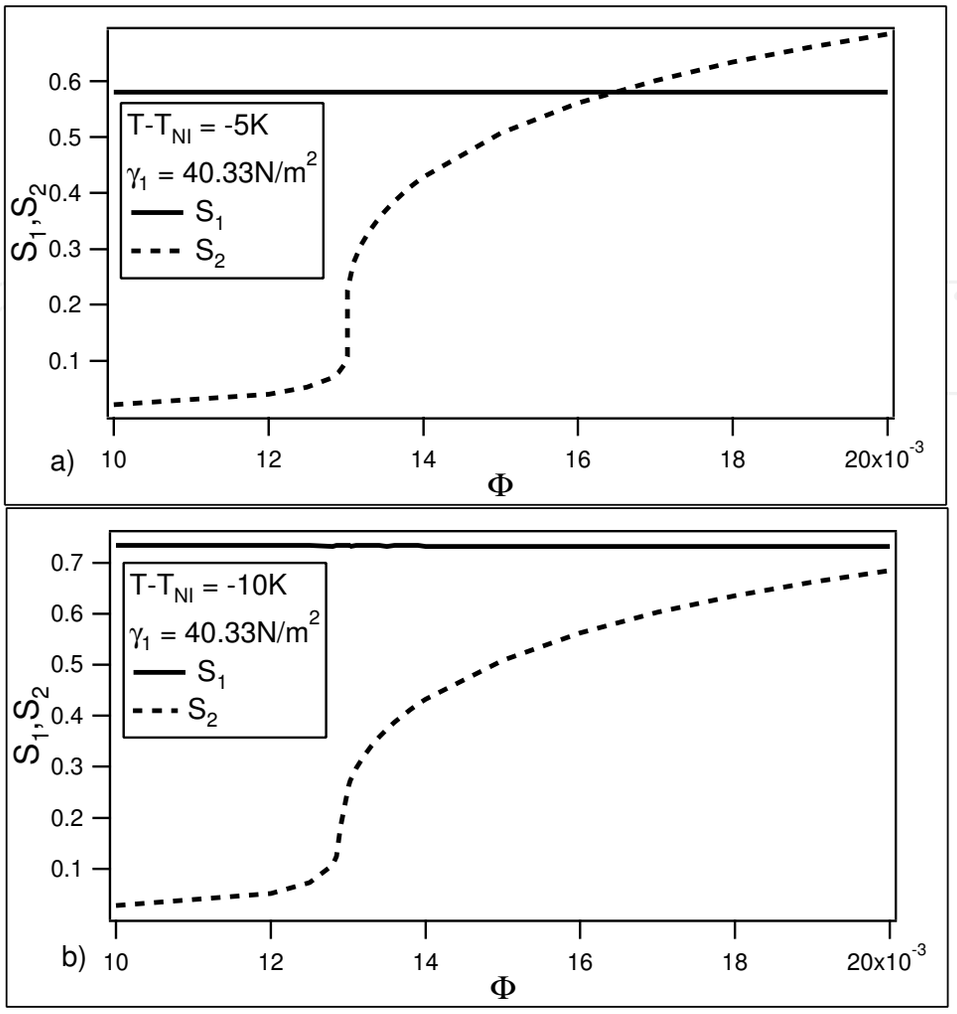


Figure 6. The order parameter variations for two temperatures lower than T_{NI} in the *subcritical* regime.

continuous, the order parameter is continuous at the transition. In both figures, the order parameter of the liquid crystal is constant. Therefore the CNTs are enslaved by LC. The degree of ordering of CNTs is present even at small volume fractions, so that the CNTs are in the paranematic phase.

In Figure 7, the temperature is greater than nematic-isotropic phase transition temperature, so that the LC is in the isotropic phase (even if the degree of ordering exists it is very small and can not be seen on the figure). For low volume fraction, the CNTs are in the isotropic phase and becomes nematic by a first order phase transition at some value of Φ.

The phase diagram for the monodisperse system in the *supercritical* regime, for $L_2 = 200$ and $L_2 = 400$, respectively is shown in Figure 8.

For a more realistic value of the coupling constant $\gamma_1 >> \gamma_1^{(c)}$, in the nematic phase of LC, there is only a gradual variation of the order parameter of CNTs with the volume fraction and temperature. Above T_{NI}, the transition isotropic-nematic of CNTs is first order and also an induced first order isotropic-paranematic phase transition takes place in LC. With increasing temperature, the transitions takes place at a larger volume fractions. For longer CNTs, the volume fractions at the transition are lower.

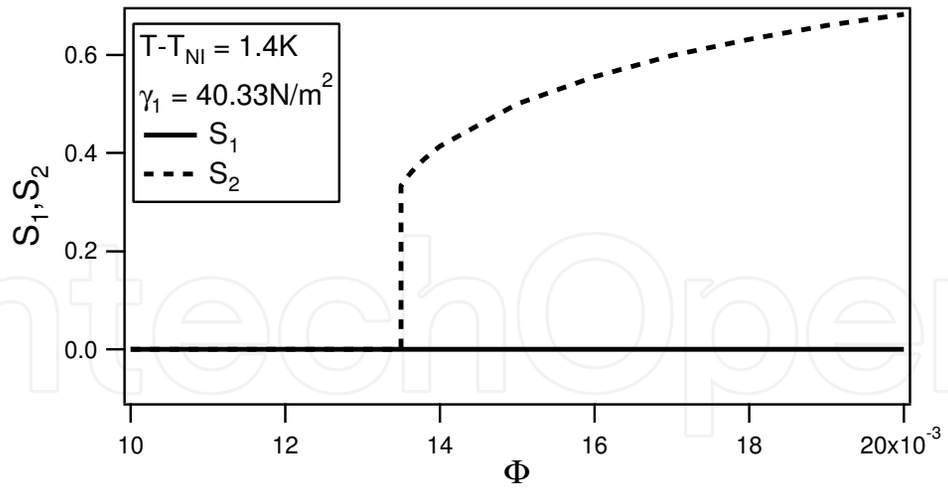


Figure 7. The order parameter variations for a temperature larger than T_{NI} in the *subcritical* regime.

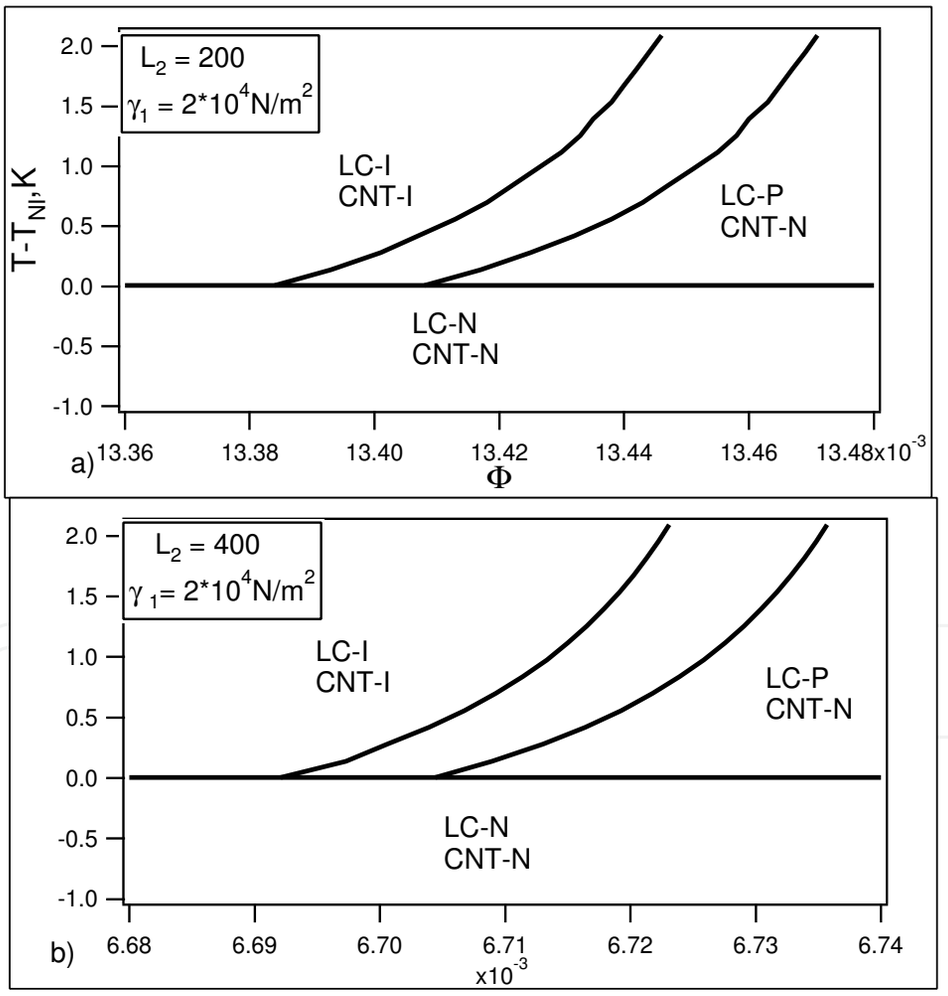


Figure 8. The (T, Φ) phase diagram of a monodisperse system in the *supercritical* regime. Signification of I, P, and N as in Figure 5.

http://dx.doi.org/10.5772/50896

3.3.2. Bidisperse CNTs

The (Φ_3, Φ_2) phase diagram of the bidisperse CNTs suspension in the LC in the *subcritical regime* is shown in Figure 9. In Figure 6a, the LC is in the nematic phase ($T - T_{NI} = -0.42$K), while in Figure 9b, the LC is in the isotropic phase ($T - T_{NI} = 1.4$K). Thick lines indicates phase boundary, while the thin lines connects the coexisting pairs (Φ_{2p}, Φ_{3p}) and (Φ_{2n}, Φ_{3n}).

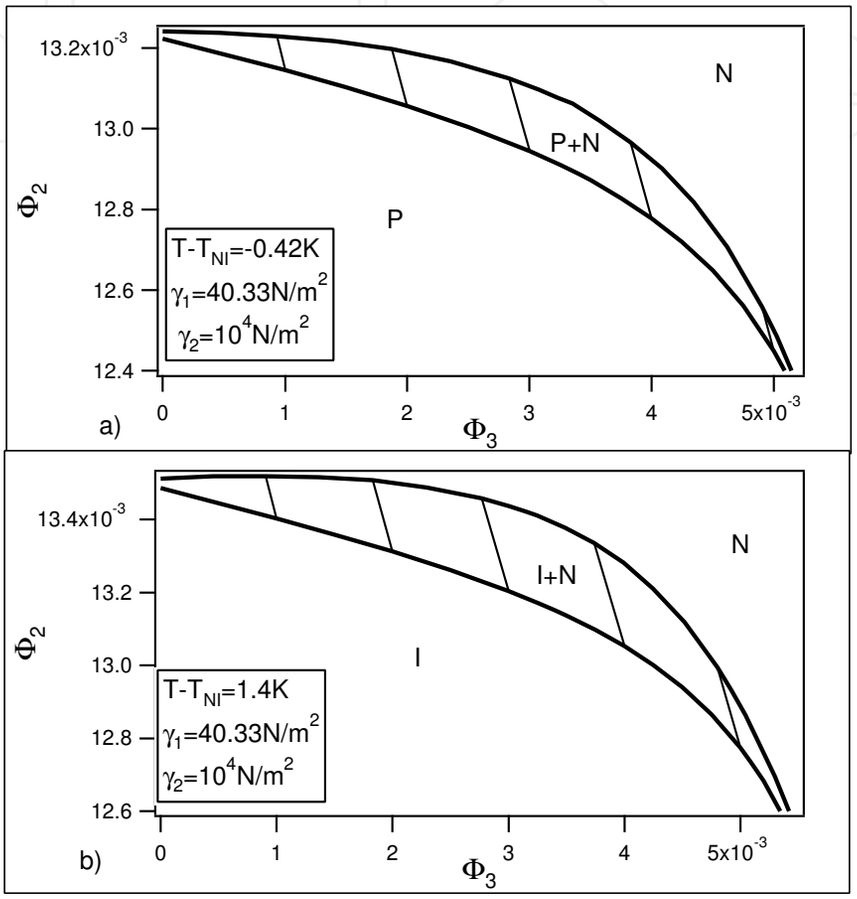


Figure 9. The (Φ_3, Φ_2) phase diagram in the *subcritical* regime for the bidisperse system, in nematic and isotropic phase of LC, respectively. I-isotropic,P-paranematic, and N-nematic.

The Figure 6 reveals two qualitatively different regimes, to which we refer as *decoupled* and *coupled* regime, respectively. In the *decoupled* regime defined by the conditions $\Phi_3 \to 0$ and $\Phi_2 \to 0$, respectively, the system exhibits monodisperse-type behavior. In the limit of very low volume fraction of the longer CNTs ($\Phi_3 \to 0$), the system is monodisperse containing only one species of CNTs of length $L_{02} = 400$ nm. In the limit of very low volume fraction of the shorter CNTs ($\Phi_2 \to 0$), the system is monodisperse containing only one species of CNTs of length $L_{03} = 800$ nm. In these two subregions, due to very small values of Φ_3 and Φ_2, respectively, the coupling term between CNTs species (the γ_{23} term in Eq. (17)) is relatively small and the species are independent. On the contrary, in the *coupled region* (intermediate region in Figure 6), the interaction term in Eq. (17) becomes important and the two CNTs species influence each other. In this region, the volume fraction of the longer CNTs increases in the nematic phase, while that of the shorter CNTs decreases.

In the case of a more realistic value of the coupling parameter between the LC molecules and CNTs $\gamma_1 = 2 * 10^3$ N/m^2 $>> \gamma_1^{(c)}$ (*supercritical* regime, the Φ_3, Φ_2) phase diagram for the bidisperse CNTs in the isotropic phase of LC ($T - T_{NI} = 1.4$K is plotted in Figure 10.

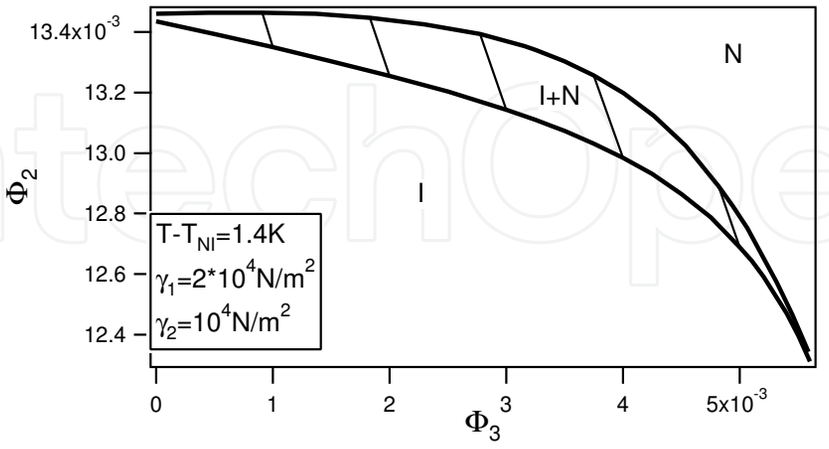


Figure 10. The (Φ_3, Φ_2) phase diagram in the *supercritical* regime for the bidisperse system, in the isotropic phase of LC, respectively. I-isotropic, and N-nematic.

The phase diagram is similar to that of Figure 9 showing again the existence of the *decoupled* and *coupled* regions that we have discussed previously.

4. Conclusions

In the paper we analyze phase behavior of mixtures consisting of LC soft carrier matrix and immersed NPs. A relatively simple phenomenological modeling is used where we focus on isotropic and nematic LC ordering.

In the first part we consider isotropic NPs. We derive the effective free energy of the mixture from which we extract the effective Flory-Huggins parameter. Its structure reveals that on entering nematic ordering phase separation is very probable. However, it could be suppressed by LC-NP interfacial contribution providing that it promotes nematic ordering. From the structure of the average elastic free energy term we also conclude that NPs have in general tendency to assemble at localized sites exhibiting relatively strong elastic distortions. We proceed by studying interaction between a nanoparticle and a topological defect, which is a typical representative of localized strong elastic distortions. It is of interest to identify conditions for which NPs could be effectively trapped to tunable localized distortions. For example, in such a way phase separation could be prevented. In addition, localized elastic distortions could be exploited controlled positional trapping of immersed NPs.

As a model system we use a cylindrical hybrid cell possessing the boojum topological defect. We consider different surface treatment of the nanoparticle and analyze where it is placed in order to minimize total free energy of the system. We find out that a nanoparticle is attracted to a region the structure of which is compatible with configuration enforced by the nanoparticle. Therefore, one could trap NPs to topological defects if its surface enforces configuration resembling the defect core structure. We further show that condensation penalty of forming defects could be in this case significantly reduced due to the *Defect Core Replacement mechanism* [3, 34].

In the second part of the paper we study interaction between nematic LC ordering and CNTs. We extend the mesoscopic model [6, 7] to include length bidispersity of CNTs dispersed in LC in the weak anchoring limit of the coupling between LC molecules and CNTs (in this limit, the coupling is dominated by the anisotropy of the surface tension not by the deformation of the director field). The main conclusions of our study can be summarized as follows:

1. Depending on the coupling between the LC molecules and CNTs (the value of the coupling constant γ_1), two different regimes can be defined: i) if $\gamma_1 < \gamma_1^{(c)}$, (the *subcritical* regime), the nematic-isotropic phase transition of CNTs dispersed in LC is first order and ii) if $\gamma_1 > \gamma_1^{(c)}$ (the *supercritical* regime), the transition is continuous. $\gamma_1^{(c)}$ is the critical value of the coupling parameter depending on the temperature (Figure 1). In both regimes, the isotropic phase of CNTs transforms into a phase with a small degree of ordering, a paranematic phase. Above the critical point this degree of orientational order is strongly increased.
2. The CNTs species are enslaved by the LC (the nematic LC order parameter depends only on the temperature not on the volume fractions of the two species).
3. The longer CNTs are driven into the nematic phase ($\Phi_{3n} - \Phi_{3p} > 0$ in Figures 6 and 7).
4. The longer CNTs induces a larger volume fractions differences $\Phi_{2n} - \Phi_{2p} > 0$ for the shorter CNTs.
5. In the nematic phase, the longer CNTs are more ordered than the shorter ones ($S_{3n} - S_{2n} > 0$).

We emphasize that the last three conclusions are similar with those obtained using the Onsager theory of nematic-isotropic phase transition of the hard rods [22–25], while the first two are specific to the dispersion of CNTs into LC.

Finally, we point out the mesoscopic model for length bidisperse CNTs dispersed in LC presented here is only a first step in considering the important influence of polydispersity on the ordering of CNTs in nematic fluids. Together with considering the attraction interaction between CNTs, this subject will be study in a future work.

Acknowledgments

V.P.-N. thanks to T. J. Sluckin for useful discussion, gratefully acknowledge the hospitality of l'Ecole Normale Supérieure de Lyon and the funding from CNRS. V.B. acknowledge support from the Romanian National Authority for Scientific Research, CNCS - UEFISCDI, project number PN-II-ID-PCE-2011-3-1007.

Author details

Vlad Popa-Nita[1,⋆], Valentin Barna[1], Robert Repnik[2] and Samo Kralj[2,3]

⋆ Address all correspondence to: v.popanita@gmail.com

1 Faculty of Physics, University of Bucharest, Bucharest, Romania
2 Laboratory Physics of Complex Systems, Faculty of Natural Sciences and Mathematics, University of Maribor, Maribor, Slovenia
3 Jožef Stefan Institute, Ljubljana, Slovenia

References

[1] A.C. Balazs, T. Emrick, T.P. Russell, Science 314, 1107 (2006).

[2] F. Li, O. Buchnev, C. Cheon, A. Glushchenko, V. Reshetnyak, Y. Reznikov, T. J. Sluckin, and J. L. West, Phys. Rev. Lett. 97, 147801 (2006).

[3] B. Rozic, V. Tzitzios, E. Karatairi, U. Tkalec, G. Nounesis, Z. Kutnjak, G. Cordoyiannis, R. Rosso, E.G. Virga, I. Musevic, S. Kralj, Eur. Phys. J. E 34, 17 (2011).

[4] P.G. de Gennes and J. Prost, The Physics of Liquid Crystals, Oxford University Press, Oxford (1993).

[5] B. Rozic, M. Jagodic, S. Gyergyek, M. Drofenik, S. Kralj, G. Lahajnar, Z. Jaglicic, Z. Kutnjak, Ferroelectrics 410, 37 (2011).

[6] P. van der Schoot, V. Popa-Nita, and S. Kralj, J. Phys. Chem. B 112, 4512 (2008).

[7] V. Popa-Nita and S. Kralj, J. Chem. Phys. 132, 024902 (2010).

[8] V. Popa-Nita, M. Cvetko and S. Kralj, in *Electronic Properties of Carbon Nanotubes*, (Edited by Jose Mauricio Marulanda (Intech, 2011).

[9] C. Zakri, Liquid Crystals Today 16, 1 (2011).

[10] S. Zhang and S. Kumar, Small 4, 1270 (2008).

[11] J. P. F. Lagerwall and G. Scalia, J. Mater. Chem. 18, 2890 (2008).

[12] M. Rahman and W. Lee, J. Phys. D: Appl. Phys. 42, 063001 (2009).

[13] M. D. Lynch and D. L. Patrick, Nano Lett. 2, 1197 (2002).

[14] I. Dierking, G. Scalia, and P. Morales, J. of Appl. Phys. 97, 044309 (2005).

[15] J. Lagerwall, G. Scalia, M. Haluska, U. Dettlaff-Weglikowska, S. Roth, and F. Giesselmann, Adv. Mater. 19, 359 (2007).

[16] N. Lebovka, T. Dadakove, L. Lysetskiy, O. Melezhyk, G. Puchkovska, T. Gavrilko, J. baran, M. Drodz, J. Molecular Structure 887, 135 (2008).

[17] M. J. Green, N. Behabtu, M. Pasquali, W. W. Adams, Polymer 50, 4979 (2009).

[18] Y. Sabba and E. L. Thomas, Macromolecules 37, 4815 (2004).

[19] A. M. Somoza, C. Sagui, and C. Roland, Phys. Rev. B63, 081403-1 (2001).

[20] M. J. Green, A. N. G. Parra-Vasquez, N. Behabtu, M. Pasquali, J. Chem. Phys. 131, 084901 (2009).

[21] W. Song and A. H. Windle, Macromolecules 38, 6181 (2005).

[22] H. N. W. Lekkerkerker, Ph. Coulon and R. Van der Haegen, J. Chem. Phys. 80, 3427 (1984).

[23] T. Odijk, Macromolecules 19, 2313 (1986).

[24] G. J. Vroege and H. N. W. Lekkerkerker, Rep. Prog. Phys. 55, 1241 (1992).

[25] H. N. W. Lekkerkerker and G. J. Vroege, J. Philos. Trans. R. Soc. London, Ser A, 344, 419 (1993).

[26] P. Kaiser, W. Wiese, and S. Hess, J. Non-Equilib. Thermodyn. 17, 153 (1992).

[27] P. J. Flory, Proc. R. Soc. A 243, 73 (1956).

[28] S. Kralj, Z. Bradac, and V. Popa-Nita, J. Phys. Condens. Matter 20, 244112 (2008).

[29] V. J. Anderson, E. M. Terentjev, S. P. Meeker, J. Crain, and W. C. K. Poon, Eur. Phys. J E 4, 11 (2011).

[30] S. Kralj, R. Rosso, and E.G. Virga, Phys. Rev. E 78, 031701 (2008).

[31] S. Kralj, R. Rosso, and E.G. Virga, Phys. Rev. E 81, 021702 (2010).

[32] D. Coursault , J. Grand , B. Zappone , H. Ayeb , G. Levi, N. Felidj , and E. Lacaze, Adv. Mater. 24, 1461 (2012).

[33] S. Kralj, E.G. Virga, S. Zumer, Phys.Rev.E 60, 1858 (1999).

[34] H. Kikuchi, M. Yokota, Y. Hisakado, H. Yang, and T. Kajiyama, Nat. Mater. 1, 64 (2002).

[35] L. Onsager, Ann. N. Y. Acad. Sci. 51, 727 (1949).

[36] M. Doi, J. Polym. Sci., Part B: Polym. Phys. 19, 229 (1981); N. Kuzuu and M. Doi, J. Phys. Soc. Jpn. 52, 3486 (1983).

[37] M. Doi and S. F. Edwards, *Theory of Polymer Dynamics* (Clarendon, Oxford, 1989).

[38] P. Oswald and P. Pieranski, *Nematic and Cholesteric Liquid crystals; concepts and physical properties illustrated by experiments* (Taylor and Francis Group, CRC Press, in Liquid Crystals Book Series, Boca Raton, 2005).

IntechOpen

IntechOpen